Extended Data

Extended Data figures and tables with legends

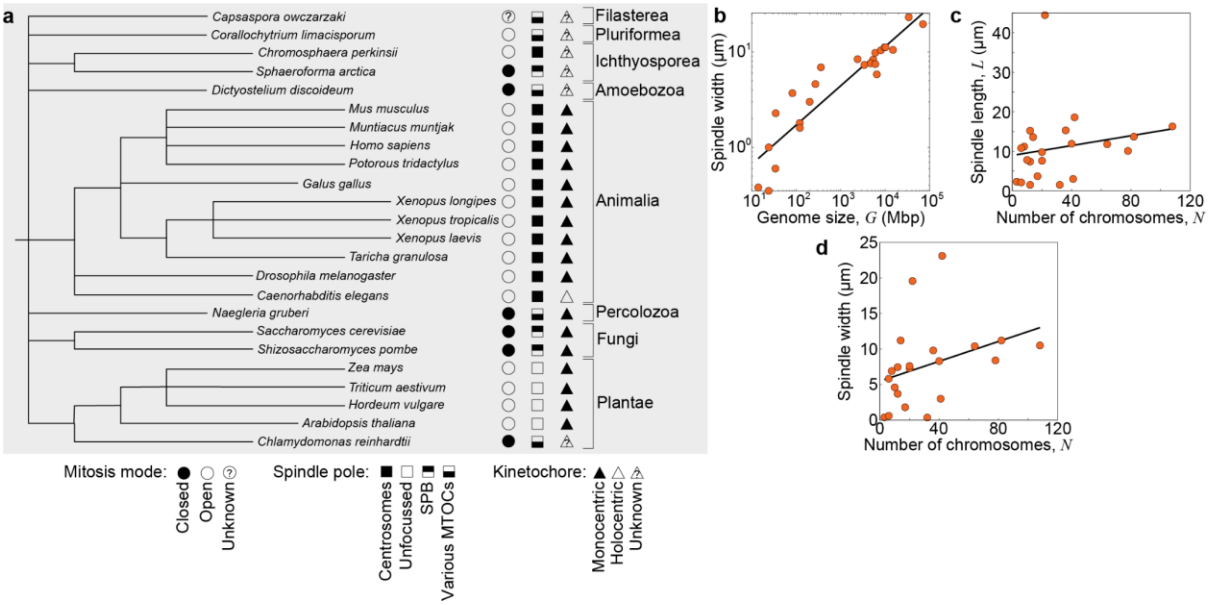

Extended Data Figure 1. Phylogenetic tree of eukaryotic species used in the study and their mitotic spindle parameters versus number of chromosomes or genome size. a, A phylogenetic tree based on the NCBI taxonomy, including species from Extended Data Table 1, with eukaryotic kingdoms, clades, or phyla denoted on the right. Schemes representing various modes of mitosis (circles), spindle pole organization (squares), and kinetochore structure (triangles) are shown according to the legend at the bottom. **b**, Spindle width as a function of the genome size for the same species as in Figure 1d, and a power-law fit with an exponent $W \propto G^{0.41}$, $R^2 = 0.85$, $p = 10^{-10}$. **c**, Spindle length, L, as a function of the chromosome number, N, for the same species as in Figure 1d, and a linear fit, $R^2 = 0.04$, $p = 0.39$. **d**, Spindle width as a function of the chromosome number, N, for the same species as in Figure 1d, and a linear fit, $R^2 = 0.12$, $p = 0.12$. Abbreviations: SPB, spindle pole body, MTOCs, microtubule-organizing centers.

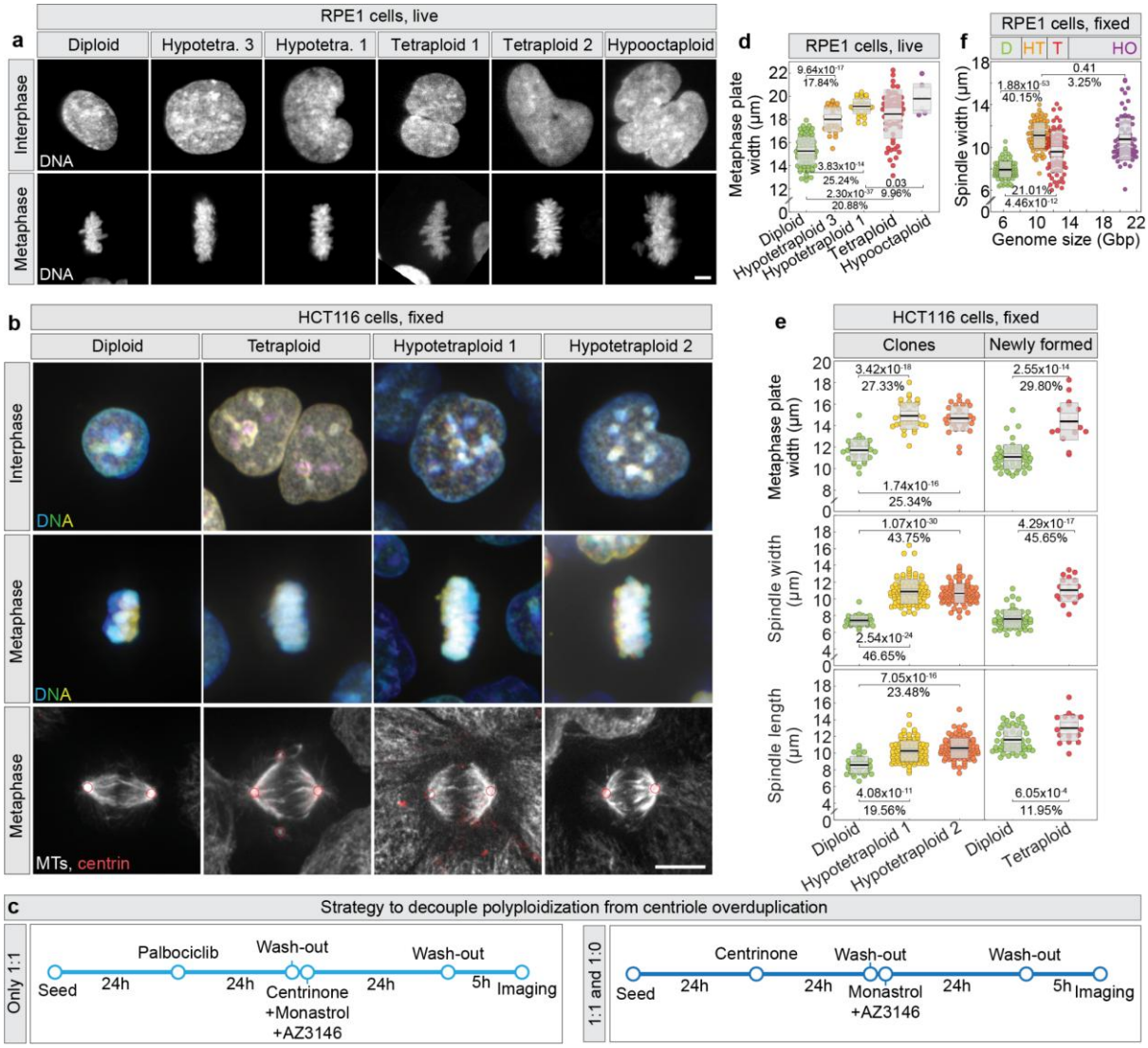

Extended Data Figure 2. The scaling of spindle dimensions with ploidy in human differentiated cells is determined by the amount of DNA in the metaphase plate. a, DNA in live-imaged RPE-1 cells of different ploidies stably expressing H2B-Dendra2 or H2B-GFP at interphase (top row) and last frame before anaphase (bottom row). **b**, DNA (color-coded for depth) in fixed HCT116 cells of different ploidies in interphase (top) and metaphase (middle). HCT116 cells of different ploidies in metaphase immunostained for α-tubulin (MTs, gray) and centrin-3 (centrioles, red, encircled) (bottom). DNA was stained with DAPI. **c**, Protocols to generate polyploid cells without centriole overduplication, targeting two outcomes: cells with one centriole per centrosome (1:1, left) or a mixture of cells with one centriole per centrosome (1:1) and cells with only a single centriole (1:0) (right). Exact concentrations are detailed in the Methods. **d**, Metaphase plate width across live-imaged RPE1 cells of different ploidies. **e**, Metaphase plate width (top), spindle width (middle) and spindle length (bottom) for fixed hypo-tetraploid HCT116 clones and their diploid controls (left), and newly formed tetraploids with their internal diploid controls (right). **f**, Spindle width across fixed RPE1 cells with different ploidies. Percentages on (d), (e) and (f) represent differences from the mean values, the thick black line shows the mean; the light and dark gray areas mark 95% confidence interval on the mean and standard deviation, respectively; p values from (Tukey's HSD test) are given in (d), (e, left) and (f); p values from (Student's t-test) are given in (e, right). Number of cells - (a) 40, 17, 21, 28; (d) 82, 36, 28, 63, 7; (e) 32, 32, 32, 54, 20 (top); 32, 96, 100, 54, 20 (middle);

32, 96, 100, 54, 20 (bottom); (f) 100, 68, 86, 75. Each group is a pool of at least three independent experiments. Abbreviations: Hypotetra. 1, hypotetraploid clone RPT1; Hypotetra. 3, hypotetraploid clone RPT3; Tetraploid 1, tetraploid cell generated by cytokinesis failure; Tetraploid 2, tetraploid cell generated by mitotic slippage; Hypotetraploid 1, hypotetraploid clone HPT1; Hypotetraploid 3, hypotetraploid clone HPT3; D, diploid; HT, hypotetraploid; T, tetraploid; HO, hypooctaploid. All scale bars, 5 μm.

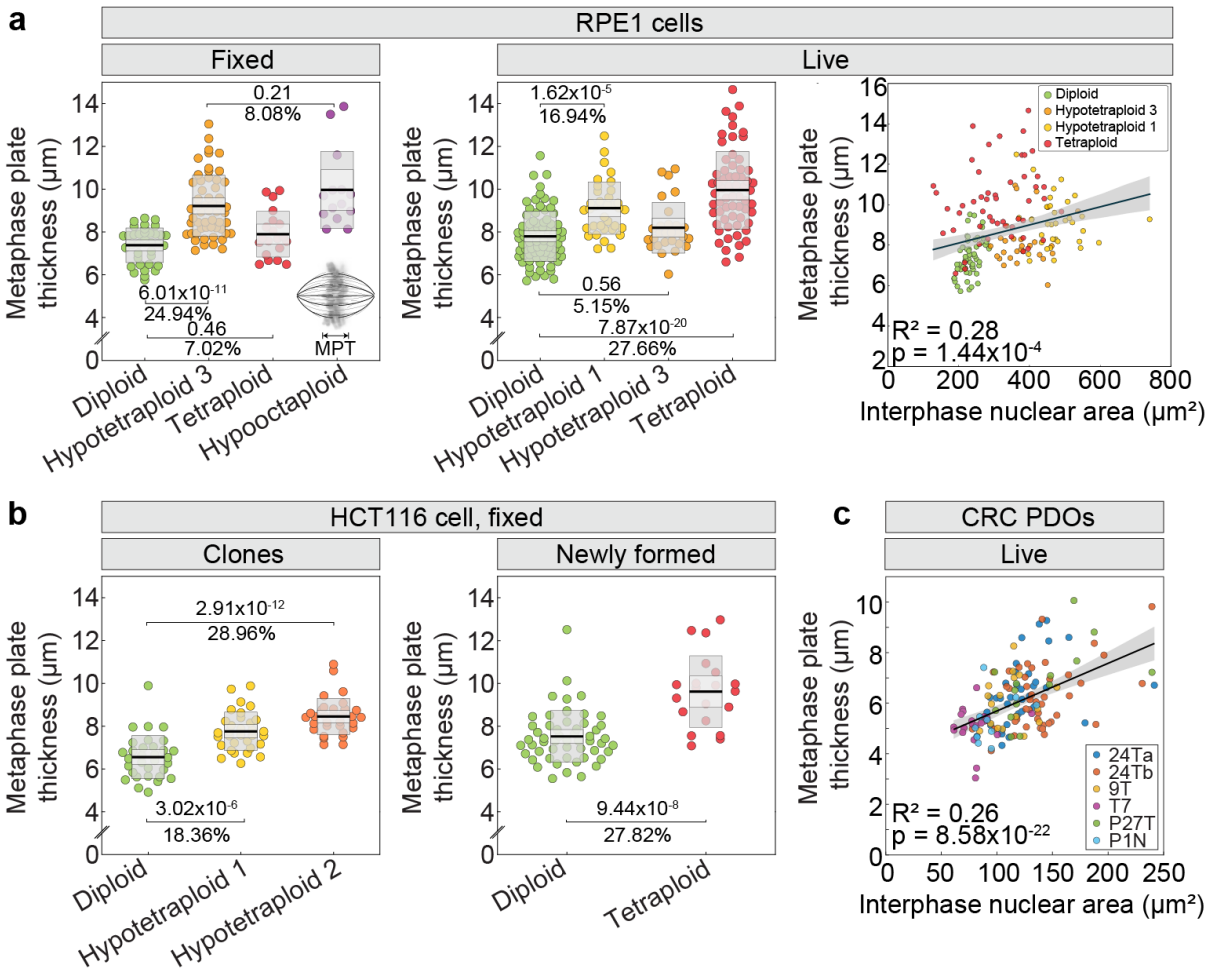

Extended Data Figure 3. Metaphase plate thickness increases with increasing ploidy in human differentiated cells and colorectal patient-derived organoids. a, Metaphase plate thickness (MPT) for RPE1 cells of different ploidies. Fixed cells (left), live cells (middle). The scheme of MPT measurement is shown in the left graph. Metaphase plate thickness versus interphase nuclear area for live-imaged RPE1 cells (right) of different ploidies for conditions as indicated in the legend. Black line represents mean linear fit; shaded area, 95% confidence interval. Metaphase plate thickness for live-imaged RPE1 cells was measured at a frame before anaphase onset. Hypotetraploids 1 and 3 represent clones RPT1 and RPT3. **b**, Metaphase plate thickness for fixed hypotetraploid HCT116 clones HTP1 and HPT2 and their diploid controls (left), and newly formed tetraploids with their internal diploid controls (right). **c**, Metaphase plate thickness versus interphase nuclear area of cells from live-imaged colorectal cancer (CRC) patient derived organoids (PDOs) across multiple lines (legend). On (a, left and middle) and (b) the black line shows the mean; the light and dark gray areas mark 95% confidence intervals on the mean and standard deviation, respectively. In (a, right) and (c), lines represent mean linear fit; shaded areas, 95% confidence interval. P values in (a, left and middle) are given from (Tukey's HSD test), in (a, right) and (c) from (Wald test) and in (b) from (Student's t test). Number of cells - (a) 37, 55, 20, 14 (left); 82, 36, 28, 63 (middle); 58, 28, 36, 51 (right); (b) 32, 32, 32 (left); 54, 20 (right); (c) 35, 44, 17, 20, 14, 10. Each group is a pool of at least three independent experiments.

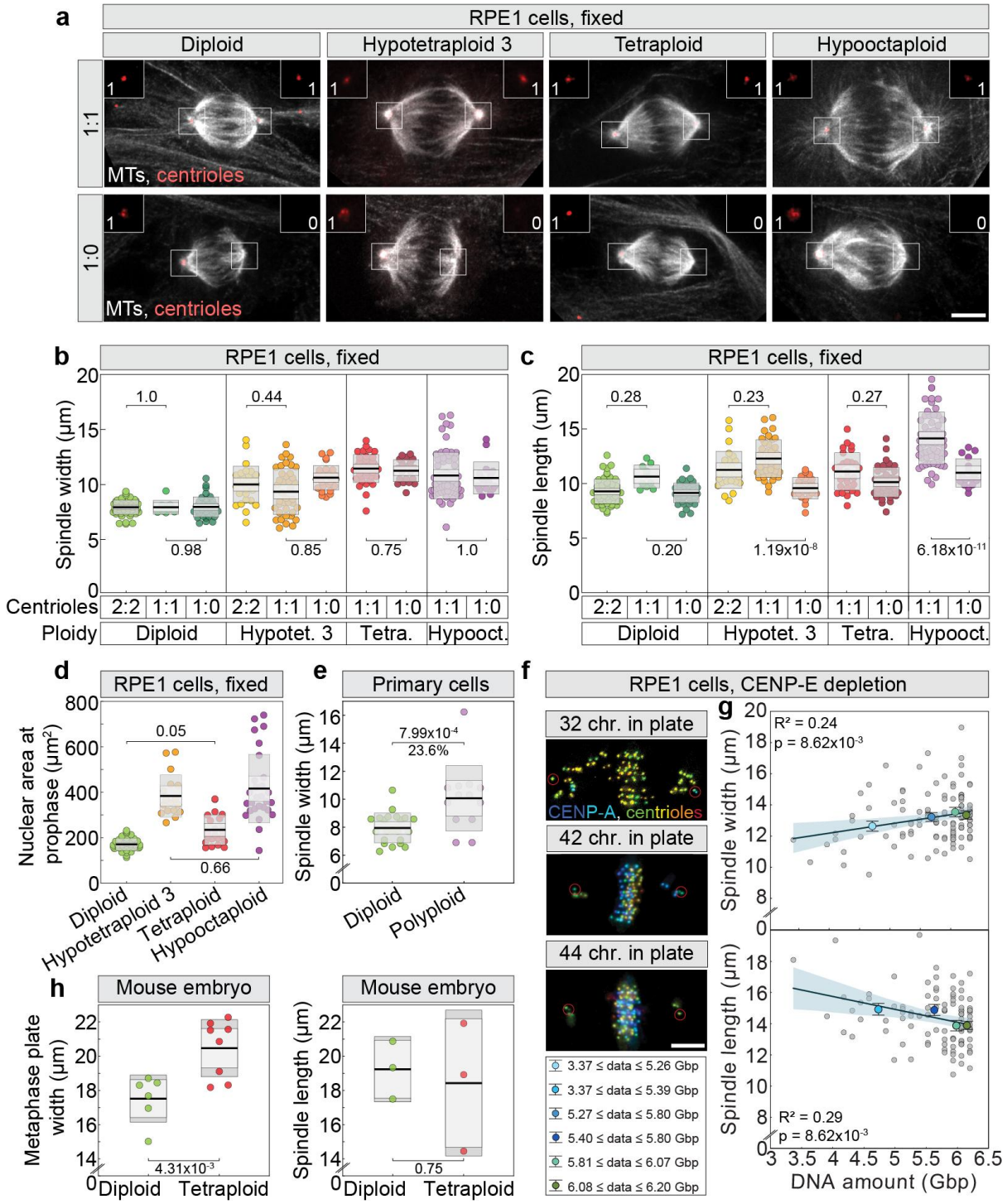

Extended Data Figure 4. Number of centrosomes impacts spindle length, but not spindle width across ploidies in differentiated cells. a, RPE1 cells of different ploidies immunostained for α-tubulin (MTs, grey) and centrin-3 (centrioles, red, encircled). First row represents spindles with one centriole on each centrosome (1:1) and the bottom row represents spindles with only one centriole (1:0). Zoomed views of the centrosome area (boxed) are located in the upper corners. **b** and **c**, Spindle width (b) and spindle length (c) across different ploidies and different number of centrioles. The black line shows the mean; the light and dark gray areas mark 95% confidence intervals on the mean and standard deviation, respectively. **d**, Nuclear area at prophase across different ploidies for fixed RPE1 cells. **e**, Spindle width across primary mouse cells of different ploidy. **f**, RPE1 cells stably expressing CENP-A-GFP (CENP-

A), and centrin-3-GFP (centrioles, encircled) color coded for depth, after depletion of CENP-E, with indicated number of chromosomes in the metaphase plate. **g**, Spindle width (top) and spindle length (bottom) versus DNA amount in metaphase plate for RPE-1 cells fixed after CENP-E depletion with mean ± standard error of the mean (SEM) for conditions as indicated in the legend. The DNA amount was determined by multiplying the total genomic DNA by the number of chromosomes retained in the metaphase plate. Black line, linear fit; blue area, 95% confidence interval. **h**, Metaphase plate width (left) and spindle length (right) for diploid and tetraploid mouse acentriolar blastocysts. Data is measured from published images[50]. P values (Tukey's HSD test) are given in (b), (c) and (d); p values from (Student's T-test) are given in (e) and (h); p values from (Wald test) are given in (g). Abbreviations: Hypotet. 3, hypotetraploid clone RPT3; Tetra., tetraploid; Hypooct., hypooctaploid; chr., chromosomes. All scale bars, 5 µm. Number of cells - (b) 55, 9, 36, 27, 38, 21, 28, 40, 60, 16; (c) 55, 10, 41, 27, 38, 22, 28, 43, 63, 16; (d) 40, 17, 21, 28; (e) 22, 13; each group is a pool of at least three independent experiments; (g) 115 (top), 105 (bottom) contain data from 2 independent experiments.

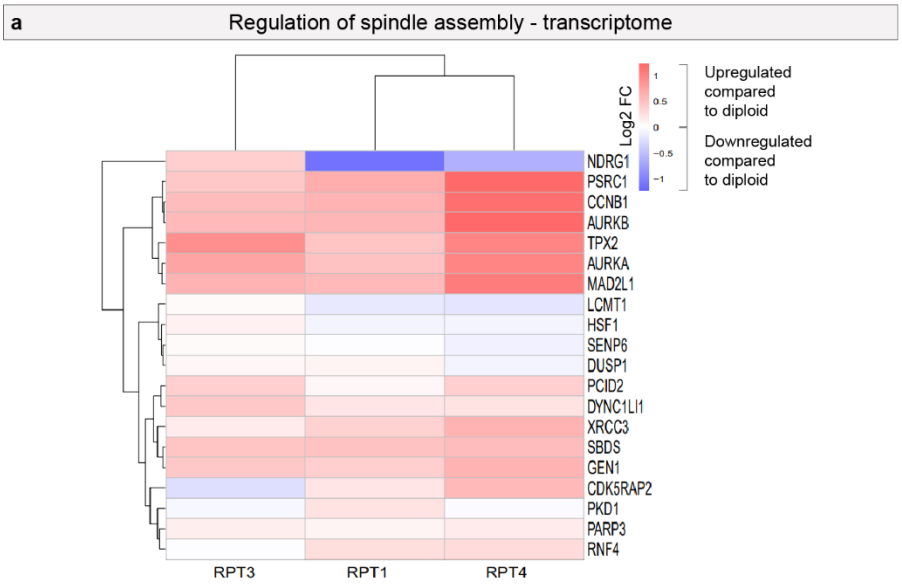
a
Regulation of spindle assembly - transcriptome
Log2 FC
Upregulated compared to diploid
Downregulated compared to diploid
NDRG1
PSRC1
CCNB1
AURKB
TPX2
AURKA
MAD2L1
LCMT1
HSF1
SENP6
DUSP1
PCID2
DYNC1LI1
XRCC3
SBDS
GEN1
CDK5RAP2
PKD1
PARP3
RNF4
RPT3
RPT1
RPT4

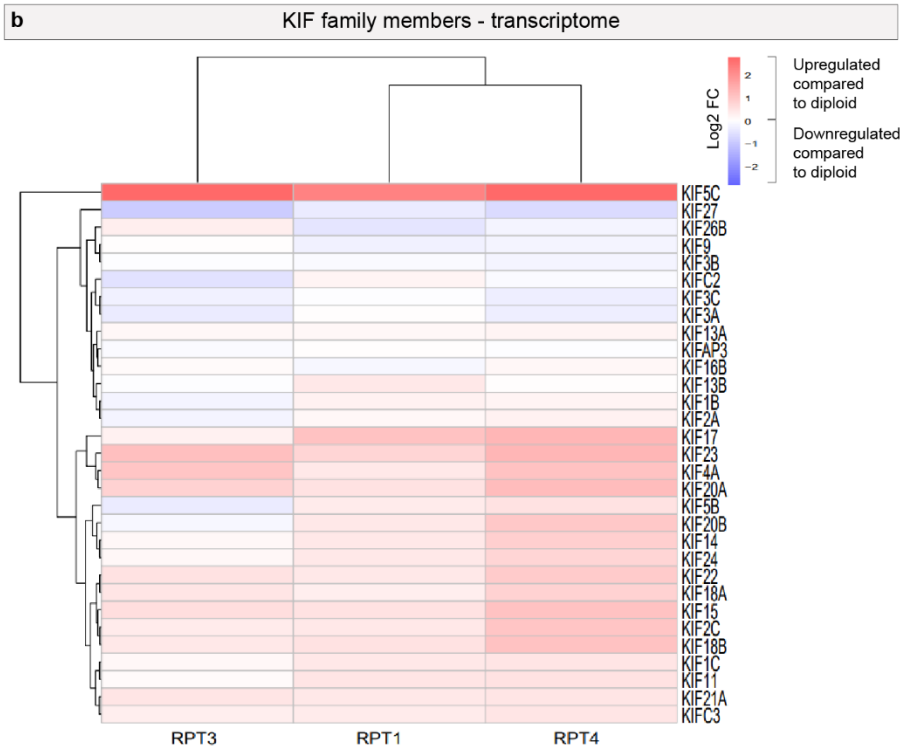
b
KIF family members - transcriptome
Log2 FC
Upregulated compared to diploid
Downregulated compared to diploid
KIF5C
KIF27
KIF26B
KIF9
KIF3B
KIFC2
KIF3C
KIF3A
KIF13A
KIFAP3
KIF16B
KIF13B
KIF1B
KIF2A
KIF17
KIF23
KIF4A
KIF20A
KIF5B
KIF20B
KIF14
KIF24
KIF22
KIF18A
KIF15
KIF2C
KIF18B
KIF1C
KIF11
KIF21A
KIFC3
RPT3
RPT1
RPT4

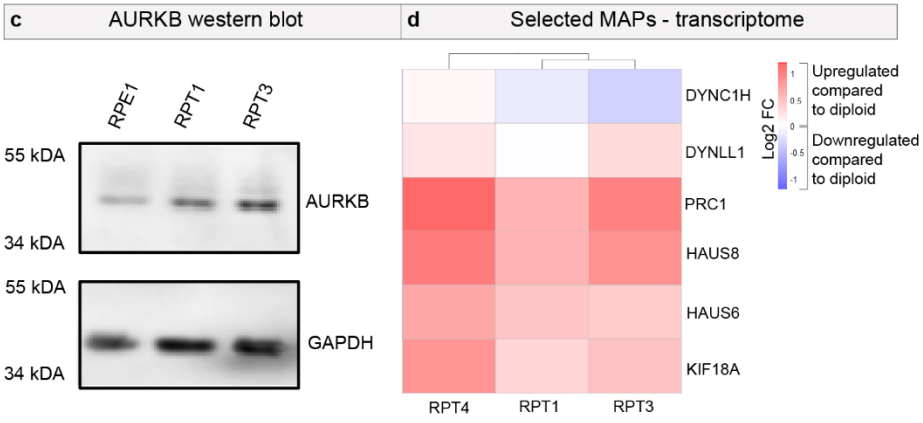
c
AURKB western blot
RPE1
RPT1
RPT3
55 kDA
34 kDA
AURKB
55 kDA
34 kDA
GAPDH
d
Selected MAPs - transcriptome
Log2 FC
Upregulated compared to diploid
Downregulated compared to diploid
DYNC1H
DYNLL1
PRC1
HAUS8
HAUS6
KIF18A
RPT4
RPT1
RPT3

Extended Data Figure 5. Transcriptome analysis of adapted tetraploid clones reveals substantial changes in the expression of mitotic factors compared to the diploid cells. a, Comparison of genes involved in spindle assembly in hypotetraploid RPE1 (RPT) cell lines and their diploid parental wild type counterparts. Genes significantly upregulated (red) and downregulated (blue) are shown (FDR < 0.05). FC, fold change. **b**, Expression changes in genes of the kinesin (KIF) family from post-tetraploid cell lines compared to the diploid parental wild type. GOCC annotation highlights the functional relevance of these changes, with significantly upregulated (red) and downregulated (blue) genes indicated (FDR < 0.05). GOCC annotation was employed to identify functional pathways. **c**, Immunoblot analysis of lysates from indicated cell lines. Antibody against Aurora B (AURKB) was used to estimate protein level, with glyceraldehyde-3-phosphate dehydrogenase (GAPDH) serving as the loading control. **d**, Comparison of genes coding for proteins which were perturbed on Fig. 4j in hypotetraploid RPT cell lines and their diploid parental wild type counterparts.

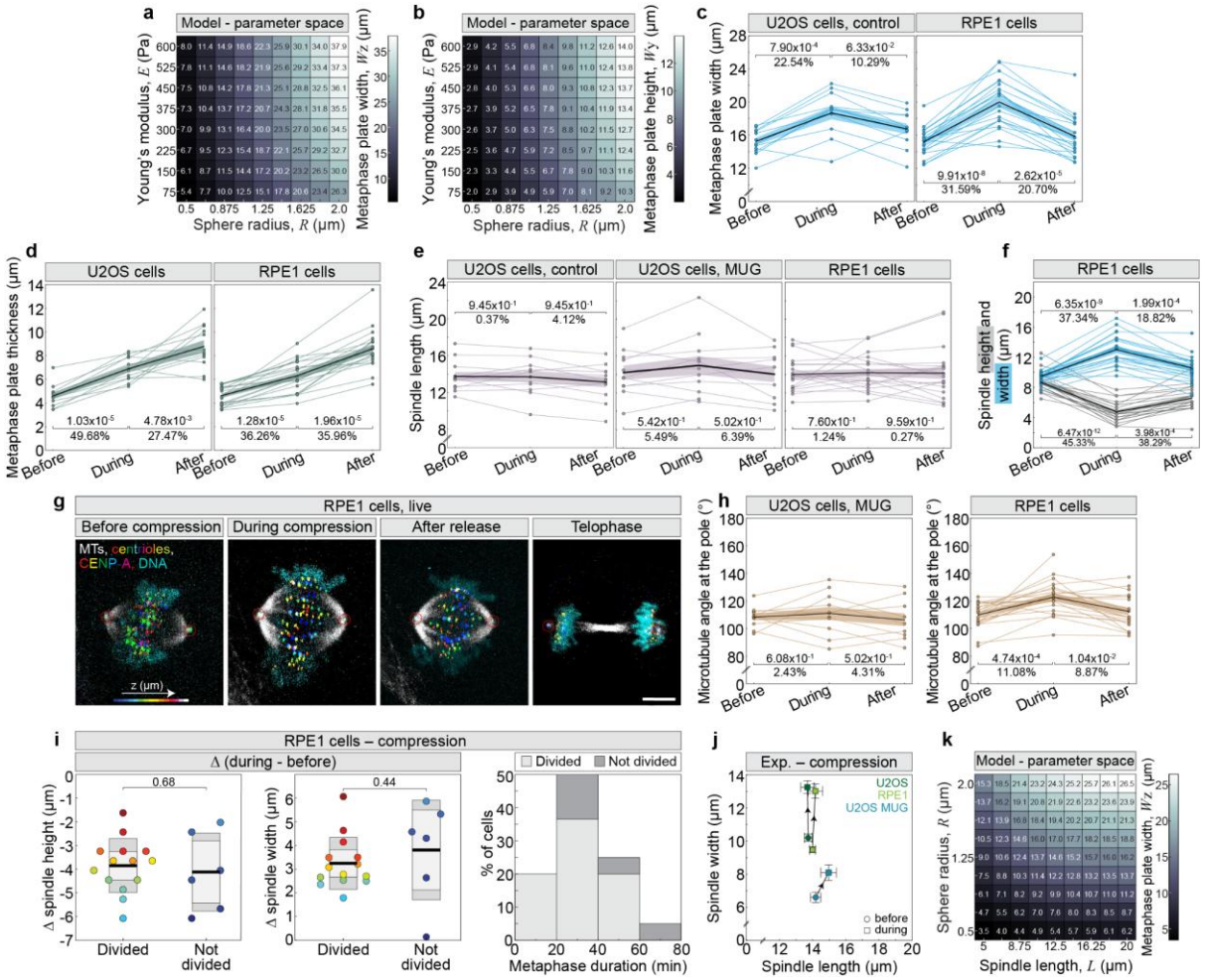

Extended Data Figure 6. Acute spindle compression increases metaphase plate width and thickness without affecting spindle length and blocking cell proliferation. a, Phase diagram of the metaphase plate width, dimension perpendicular to the direction of external force, W_z, and **b**, the metaphase plate height, dimension in the direction of external force, W_y, as a function of Young's modulus and sphere radius for compression coefficient $k = 100$ pN/μm. **c**, Metaphase plate width in U2OS control (left) and RPE1 control (right) cells for three time points related to cell compression. **d**, Metaphase plate thickness for three time points related to compression of U2OS control (left) and RPE1 control (right) cells. **e**, Spindle length for three time points related to compression of U2OS control (left), U2OS cells in mitosis with unreplicated genome (MUG) (middle) and RPE1 control (right) cells. **f**, Spindle height (magenta) and spindle width (green) for three time points related to compression of control RPE1 cells. **g**, Time-lapse of control RPE1 cells stably expressing CENP-A-GFP and centrin-GFP (centrioles, encircled) (color-coded for depth) in compression experiment, with SiR-tubulin (MTs, grey) and Hoechst 33342 labelled DNA (cyan). **h,** Angle between pole and outermost kinetochore fiber for three time points related to compression of U2OS cells in MUG (left) and control RPE1 cells (right). **i,** Changes (Δ) in height (left) and width (middle) during compression and metaphase duration histogram after compression for control RPE1 cells that either divided (light grey) or did not divide (dark grey) during imaging (right). Colored points on left and middle represent individual cells; the black line shows the mean, with light and dark

grey areas marking 95% confidence intervals for the mean and standard deviation. p-values (Student's t-test) are shown above. **j,** Mean ± SEM for spindle width versus spindle length for compression experiments; lines connect corresponding mean values before and after compression. Number of cells: 12, 11, 21. **k**, Phase diagram of metaphase plate width W_z, as a function of chromosome radius and spindle length for $k = 100$ pN/μm. In (c), (d), (e), (f) and (h) black line, mean value; shaded area, 95% confidence interval. Number of cells - (c) 12 (left); 21 (right); (d) 12 (left); 21 (right); (e) 12 (left), 21 (middle), 11 (right); (f) 21; (h) 21 (left), 11 (right); (i) 14, 6 (left); 14, 6 (middle); 20 (right); (j) 12 (left), 21 (middle), 11 (right). In (a), (b), and (k) parameters are as in (Fig. 3), unless stated otherwise. Abbreviations: Exp., experiment. Number of cells equals the number of independent experiments.

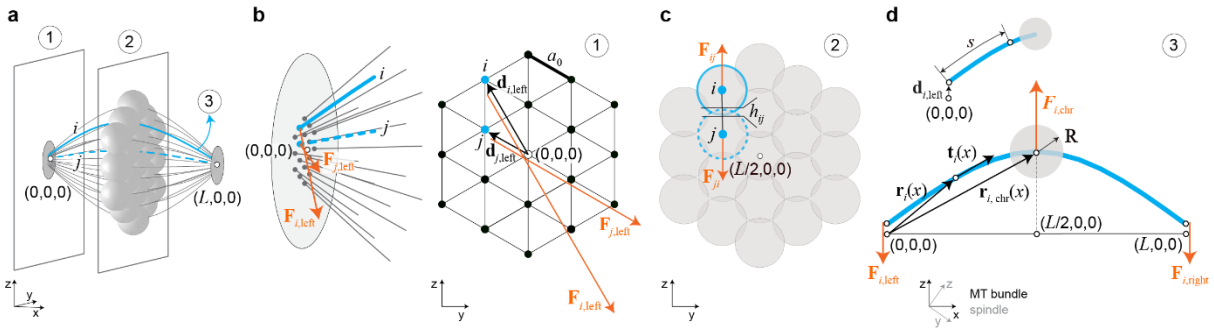

Extended Data Figure 7. Scheme of the model. a, Three-dimensional scheme of the metaphase spindle with 19 chromosomes for the parameter values from Fig. 3. Two cross-sections of the spindle which contain the left spindle pole, and the metaphase plate are numbered (1) and (2) respectively, whereas a single bundle is numbered (3). Chromosomes are shown in light gray, microtubule bundles in gray, and spindle poles in dark gray. Two individual bundles, labeled i and j, are shown by solid and dashed green lines, respectively. Coordinates of the right and left spindle poles are shown by triples of numbers. **b,** Scheme of the left spindle pole in side view (left) and end-on view (right). The forces exerted by the pole on the microtubule bundle, $F_{i,\mathrm{left}}$ and $F_{j,\mathrm{left}}$, are shown in orange for bundles i and j, respectively. The positions of the left microtubule bundle ends are shown as green dots for the bundles i and j, and as black dots for the other bundles. The radius vectors for the left microtubule ends, $d_{i,\mathrm{left}}$ and $d_{j,\mathrm{left}}$, are shown in black. The coordinate of the left spindle pole is shown by a triple of numbers. The lattice parameter, a_0, is shown in the end-on view. **c,** Scheme of the metaphase plate in end-on view. The repulsive forces F_{ij} and F_{ji} mutually exerted between the bundles i and j, respectively, are shown in orange. The reduction of distance, h_{ij}, between the chromosomes corresponding to bundles i and j is shown in black. The coordinate of the metaphase plate center is shown by a triple of numbers. **d,** Scheme of the microtubule bundle i. The forces exerted by the pole on the left and right ends of microtubule bundles, $F_{i,\mathrm{left}}$ and $F_{i,\mathrm{right}}$ respectively, as well as the repulsive force exerted by the neighboring chromosomes, $F_{i,\mathrm{chr}}$, are shown in orange. The radius vector at the coordinate x, $r_i(x)$, the tangent, $t_i(x)$, the radius vector of the chromosome, $r_{i,\mathrm{chr}}(x)$, and the radius of the chromosome, R, are shown in black. The coordinates of the left and right poles, as well as the center of the metaphase plate, are shown by triples of numbers. The contour length for bundle i is shown in the inset. The coordinate systems of the entire spindle and its individual components are shown in insets within each panel.

Extended Data Table 1. Measurements of metaphase plate width, spindle length, and spindle width from published images of mitotic spindles in eukaryotes with diverse ploidy levels, genome sizes, and chromosome numbers.

Species	Cell type and ploidy	Genome size (Mbp)	Chromosome number	Spindle length (μm)	Spindle width (μm)	Plate width (μm)	References for genome size and chromosome number	References for spindle length and width	References for metaphase plate width
Shizosaccharomyces pombe	Haploid	14	3	2.3	0.38	2.9	NCBI GenBank	(106)	(107)[a]
Saccharomyces cerevisiae	Diploid	24	32	1.5	0.35	2.3	NCBI GenBank	(108)	(109)[a]
Corallochytrium limacisporum	Unknown, assumed diploid	24.1	Unknown	1.9	1.0	1.8	(110)	(111, Extended data Fig. 9C)[b]	(111, Extended data Fig. 9C)[b]
Capsasphora owczarzaki	Unknown, assumed diploid	27.9	Unknown	1.5	Unknown	1.6	(110)	(112, Fig. 2B)[b]	(112, Fig. 2B)[b, c]
Dictyostelium discoideum	Haploid	34	6	2.1	0.6	3.0	(113)	(114)	(115)[a]
Chromosphaera perkinsii	Unknown, assumed diploid	34.6	Unknown	3.91	2.28	2.5	(110)	(111)	(111)
Creolimax fragrantissima	Unknown, assumed diploid	42.9	Unknown	2.4	1.2	Unknown	(110)	(111, Fig. 4A)[b]	Not found
Naegleria gruberi	Diploid	82	12	7.4	3.7	4.2	(113)	(116)	(116, Fig. 4)[b]
Chlamydomonas reinhardtii	Haploid	120	17	3.70	1.80	3.4	NCBI GenBank	(117)	(118, Fig. 7)[b, c]
Sphaeroforma arctica	Unknown, assumed diploid	120.9	Unknown	3.45	1.6	4.7	(110)	(111, Fig. 2C, Fig. 2D)[b]	(111)[a]
Caenorhabditis elegans	Embryo, 200-cell stage, diploid	200	41	3.0	3.0	3.3	NCBI GenBank	(18)	(18)
Drosophila melanogaster	S2 cells, diploid	260	8	11.2	6.9	8.0	NCBI GenBank	(59, Fig. 2B)[b]	(59, Fig. 1C)[b]
Arabidopsis thaliana	Root tips cell, diploid	270	10	7.8	4.6	6.9	NCBI GenBank	(119, Fig. 3)[b]	(120)
Galus gallus	DT40 B lymphocyte, diploid	2400	78	10.1	8.4	10.8	NCBI GenBank	(121, Fig. 2a)[b]	(121, Fig. 2a)[b]
Xenopus tropicalis	Embryo, stage 36, diploid	3400	20	9.8	7.3	11.3	(20)	(20, Fig. S4E, Fig. 4C)[b]	(20, Fig. S4E)[b]
Zea mays	Root tip cell, diploid	4730	20	7.6[e]	7.6	10.7	NCBI GenBank	(122)	(122)
Mus musculus	mESC, diploid	5380	40	11.9	8.3	12.1	(19)	(19)	(19)
Xenopus laevis	Embryo, stage 36, allotetraploid	6000[d]	36	15.3	9.8	14.8	(20)	(20, Fig. 4C)[b]	(20, Fig. S4E)[b]
Potorous tridactylus	Ptk1, diploid	6025	12	15.21	7.45	15.95	Animal genome size database	(123, Fig 1a)[b]	(124, Fig. 2E)[b]
Muntiacus muntjak	Fibroblast, diploid	6494	6	10.82	5.82	15.65	(125)	(126, Fig. S2A, Fig. S2A')[b]	(127, Fig. 3A)[b], (126, Fig. 1A)[b]
Homo sapiens	HEK293, hypotriploid	8000	64, modal	11.8	10.4	14.2	(19)	(19)	(19)
Homo sapiens	HeLa, hypertriploid	9720	82, modal	13.7	11.2	15.1	(19)	(19)	(19)
Hordeum vulgare	Root tip cell, diploid	10200	14	13.6[e]	11.2	15.9	NCBI GenBank	(122)	(122)
Xenopus longipes	Embryo, stage 36, dodecaploid	15000[d]	108	16.3	10.5	17.5	(20)	(20, Fig. 4C)[b]	(20, Fig. S4E)[b]
Triticum aestivum	Root tip cell, allohexaploid	34000	42	18.6[e]	23.1	27.2	NCBI GenBank	(122)	(122)
Taricha granulosa	Lung cell, diploid	70959	22	44.98	19.57	40.35	Animal genome size database	(128, Fig. 1, 2)[b], (129, Fig. 1B)[b], (130, Fig. 2)[b]	(128, Fig. 1, 2)[b], (129, Fig. 1B)[b], (130, Fig. 2)[b]

Values for spindle and genome parameters across different species with references. Superscripts: a, DNA fills the nucleus; b, measured or estimated from given figures; c, spindle has a discernible metaphase plate; d, genome size normalized to *X. tropicalis*, e, spindle with unfocused poles.

Extended Data Table 2. Measurements of metaphase plate width and spindle length from published images of acentriolar mitotic and meiotic spindles across different species and ploidy levels.

Species and system	Ploidy and stage	Metaphase plate width (µm)	Spindle length (µm)	References
Human HAP1 cells	Near-haploid	9.65	7.98	(41)
	Diploid	11.42	8.20	(41)
Human oocytes	Metaphase I	15.53 ± 1.83	13.7 ± 1.05	(43, 45, 46, 48)
	Metaphase II	11.55 ± 1.10	12.77 ± 1.08	(43, 45, 46, 48)
Mouse oocytes	Metaphase I	14.96 ± 3.11	18.95 ± 2.97	(44, 47)
	Metaphase II	9.97 ± 1.68	17.87 ± 1.74	(44, 47)
Mouse acentriolar blastocysts	Diploid[1]	17.52 ± 0.51	19.23 ± 0.80	(50)
	Tetraploid[1]	20.47 ± 0.55	18.43 ± 1.77	(50)
Porcine oocytes	Diploid metaphase II	6.49	6.40	(49)
	Tetraploid metaphase II	8.19	7.03	(49)

Data are presented as a single value, when only one data point was available, or mean ± SEM, when more data points were analyzed. Superscripts: 1, includes data from 8-cell control and 4-cell tetraploid embryos, as well as 16-cell control and 8-cell tetraploid embryos. Tetraploid mouse acentriolar blastocysts contained both binuclear and mononuclear cells. See references for detailed protocols.

Extended Data movie legends

Extended Data Movie 1. Diploid RPE1 cells and its derivatives of different ploidies during interphase and mitosis. The combined movie shows live-cell imaging of the following: a diploid RPE-1 cell expressing H2B-GFP (modal chromosome number = 46); a hypotetraploid RPT1 cell expressing H2B-GFP (modal chromosome number = 80); a newly generated mononuclear tetraploid cell with p53 knockdown expressing H2B-Dendra2 (modal chromosome number = 92); and a newly generated mononuclear hypooctaploid cell expressing H2B-GFP (modal chromosome number = 160). Tetraploid and hypooctaploid cells were generated using the procedure detailed in Extended Data Figure 2c and the Methods section. The movie plays at 7 frames per second. To ensure consistency, the first, second, and fourth segments include duplicate final frames of metaphase to match the number of frames in the third segment.

Extended Data Movie 2. Acute compression of untreated spindles and spindles with unreplicated genomes in U2OS cells. The combined movie shows live-cell imaging of z-stacks from hypertriploid U2OS cells expressing CENP-A-GFP (magenta), α-tubulin-mCherry (gray), and stained with Hoechst-DNA (cyan) under the following conditions: untreated control before compression (top left), mitosis with unreplicated genome (MUG) before compression (bottom left), untreated control during compression (top middle), MUG during compression (bottom middle), untreated control after compression (top right), and MUG after compression (bottom right). MUG cells were generated using the procedure detailed in the Methods section. All z-stacks include the same number of slices, with the 0 point defined at the center of the mitotic spindle. The movie plays at 7 frames per second.

Extended Data references

106. Ding, R., McDonald, K. L. & McIntosh, J. R. Three-dimensional reconstruction and analysis of mitotic spindles from the yeast, Schizosaccharomyces pombe. *J. Cell Biol.* **120**, 141–151 (1993).
107. Zareiesfandabadi, P. & Elting, M. W. Force by minus-end motors Dhc1 and Klp2 collapses the *S. pombe* spindle after laser ablation. *Biophys. J.* **121**, 263–276 (2022).
108. Winey, M. *et al.* Three-dimensional ultrastructural analysis of the Saccharomyces cerevisiae mitotic spindle. *J. Cell Biol.* **129**, 1601–1615 (1995).
109. Verdaasdonk, J. S., Gardner, R., Stephens, A. D., Yeh, E. & Bloom, K. Tension-dependent nucleosome remodeling at the pericentromere in yeast. *Mol. Biol. Cell* **23**, 2560–2570 (2012).
110. Grau-Bové, X. *et al.* Dynamics of genomic innovation in the unicellular ancestry of animals. *eLife* **6**, e26036 (2017).
111. Shah, H. *et al.* Life-cycle-coupled evolution of mitosis in close relatives of animals. *Nature* **630**, 116–122 (2024).
112. Pérez-Posada, A., Dudin, O., Ocaña-Pallarès, E., Ruiz-Trillo, I. & Ondracka, A. Cell cycle transcriptomics of Capsaspora provides insights into the evolution of cyclin-CDK machinery. *PLoS Genet.* **16**, e1008584 (2020).
113. Fritz-Laylin, L. K. *et al.* The genome of Naegleria gruberi illuminates early eukaryotic versatility. *Cell* **140**, 631–42 (2010).
114. Moens, P. B. Spindle and kinetochore morphology of Dictyostelium discoideum. *J. Cell Biol.* **68**, 113–122 (1976).
115. Catalano, A. & O'Day, D. H. Rad53 homologue forkhead-associated kinase A (FhkA) and Ca2+-binding protein 4a (CBP4a) are nucleolar proteins that differentially redistribute during mitosis in Dictyostelium. *Cell Div.* **8**, 4 (2013).
116. Velle, K. B. *et al.* Naegleria's mitotic spindles are built from unique tubulins and highlight core spindle features. *Curr. Biol.* **32**, 1247-1261 e6 (2022).
117. O'Toole, E., Morphew, M. & McIntosh, J. R. Electron tomography reveals aspects of spindle structure important for mechanical stability at metaphase. *Mol. Biol. Cell* **31**, 184–195 (2020).
118. Esparza, J. M. *et al.* Katanin localization requires triplet microtubules in Chlamydomonas reinhardtii. *PLoS One* **8**, e53940 (2013).
119. Ambrose, J. C. & Cyr, R. The Kinesin ATK5 Functions in Early Spindle Assembly in Arabidopsis. *Plant Cell* **19**, 226–236 (2007).
120. Romeiro Motta, M. *et al.* B1-type cyclins control microtubule organization during cell division in Arabidopsis. *EMBO Rep.* **23**, e53995 (2022).
121. Ribeiro, S. A. *et al.* Condensin Regulates the Stiffness of Vertebrate Centromeres. *Mol. Biol. Cell* **20**, 2371–2380 (2009).
122. Zhang, H. & Dawe, R. K. Total centromere size and genome size are strongly correlated in ten grass species. *Chromosome Res.* **20**, 403–412 (2012).
123. Wan, X., Cimini, D., Cameron, L. A. & Salmon, E. D. The coupling between sister kinetochore directional instability and oscillations in centromere stretch in metaphase PtK1 cells. *Mol. Biol. Cell* **23**, 1035–1046 (2012).

124. O'Connell, C. B. & Khodjakov, A. L. Cooperative mechanisms of mitotic spindle formation. *J. Cell Sci.* **120**, 1717–1722 (2007).
125. Plačková, K., Bureš, P. & Zedek, F. Centromere size scales with genome size across Eukaryotes. *Sci. Rep.* **11**, 19811 (2021).
126 Almeida, A. C. *et al.* Augmin-dependent microtubule self-organization drives kinetochore fiber maturation in mammals. *Cell Rep.* **39**, 110610 (2022).
127. Drpic, D. *et al.* Chromosome Segregation Is Biased by Kinetochore Size. *Curr. Biol.* **28**, 1344-1356.e5 (2018).
128. Mitchison, T. J. & Salmon, E. D. Poleward kinetochore fiber movement occurs during both metaphase and anaphase-A in newt lung cell mitosis. *J. Cell Biol.* **119**, 569–582 (1992).
129. Waters, J. C., Skibbens, R. V. & Salmon, E. D. Oscillating mitotic newt lung cell kinetochores are, on average, under tension and rarely push. *J. Cell Sci.* **109**, 2823–2831 (1996).
130. Rieder, C. L. & Khodjakov, A. Mitosis Through the Microscope: Advances in Seeing Inside Live Dividing Cells. *Science* **300**, 91–96 (2003).